WATER CONTENT OF PERIDOTITE XENOLITHS FROM KAAPVAAL CRATON KIMBERLITES: IMPLICATIONS ON BARREN NATURE OF KIMBERLITES

Sahroz **Khan**[1], Nóra **Liptai**[2,3], István J. **Kovács**[2,3], Yana **Fedorchuk**[4], Tivadar **M. Tóth**[1]

[1] Department of Mineralogy, Geochemistry and Petrology, University of Szeged, Egyetem Str. 2, 6722 Szeged, Hungary

[2] MTA FI Lendület Pannon LitH_2Oscope Research Group, Institute of Earth Physics and Space Science, Sopron, Hungary

[3] Institute of Earth Physics and Space Science, Eötvös Loránd Research Network, Sopron, Hungary

[4] Department of Earth and Environmental Sciences, Dalhousie University, Halifax, Nova Scotia B3H 4R2, Canada

e-mail: sahroz.khan21@gmail.com

Hydrogen abundance (commonly called water) in the nominally anhydrous mantle minerals has been extensively analyzed to determine relative ascent rates for economic kimberlite magmas and extended to comment on diamond preservation. However, the H_2O distribution and estimation studies include very few uneconomic kimberlites. In this study, we analyze hydrogen abundance in olivine, orthopyroxene, clinopyroxene and garnet in 11 xenoliths from three barren (Matsoku, Thaba Putsoa and Pipe 200) and one economic kimberlite (Bultfontein) in the Kaapvaal craton using Fourier-transform infrared (FTIR) spectroscopy. All xenoliths are harzburgites with spinel and/or garnet. Primary clinopyroxene occurs in few xenoliths. In others, clinopyroxene occurs as a metasomatic reaction product of garnet breakdown, forming an assemblage of spinel, clinopyroxene and phlogopite and are affected by partial melting. All xenoliths show protogranular texture except one from Bultfontein showing porphyroclastic texture. The FTIR spectroscopy of olivine shows absorption peaks mainly in Group 1A (P >2 GPa) pressure of hydrogenation. The garnets show peaks for only contamination and are assumed to be dry. The H_2O concentration of olivine (17–61 ppm), orthopyroxene (21–175 ppm), and clinopyroxene (87–833 ppm) were determined using the method of Kovács et al. (2008) for unoriented grains. The water distribution coefficient between orthopyroxene and olivine in kimberlite xenoliths defines two trends. These trends can also be differentiated using the pressure estimates of kimberlite xenoliths wherein all the studied barren kimberlites fall in the lower equilibration pressure trend ($D_{H2O}^{opx/ol}$ = ~ 1.0 to 9.1). Furthermore, within the low P trend, the difference between the diamond-bearing and barren kimberlites is apparent in uneconomic kimberlites' lower olivine and orthopyroxene H_2O content. This lower H_2O content could be attributed to metasomatism or subsequent dehydration events during partial melting keeping also the extremely high values for both $D_{H2O}^{melt/ol}$ and $D_{H2O}^{melt/opx}$ in mind. The petrographic signatures of partial melting and low water content of orthopyroxene and olivine with the melt hint towards dehydration of the barren kimberlite. Therefore, analyses of water content have potential in kimberlite diamond preservation determination.

1. Introduction

Hydrogen in the earth's mantle occurs as structurally bound hydroxyl (OH^-) in nominally anhydrous minerals (NAMs; Bell et al., 1992). The H contents in these nominally anhydrous minerals is reported as ppm H_2O by weight and can reach up to hundreds of ppm H_2O (Peslier, 2010). It is known to affect the physio-chemical properties of mantle rocks such as melting temperature, thermal/electrical conductivity, deformation properties, etc (Patkó et al., 2019 and references therein). It is also known to be the dominant component of volatiles in the mantle fluids which are known to accentuate the diamond dissolution. Wherein, the CO_2 and H_2O produce different dissolution features and water content affects the morphology (Fedortchouk et al., 2007; Khokhryakov, Palyanov, 2010). Mantle xenoliths entrained by the fast ascending magmas (especially, kimberlite) provide an opportunity to study the H distribution patterns and its contents of the mantle because of inadequate time for complete diffusion of H. Many articles have tried to compute the water content of continental lithosphere using the xenoliths entrained by kimberlites from cratonic setting (Bell, Rossman 1992; Kurosawa et al., 1997; Grant et al., 2007; Peslier, 2010; Baptiste et al., 2012; Peslier et al., 2012, 2017; Schmädicke et al., 2013; etc.). However, the calculated water concentration in Kaapvaal craton kimberlites spreads over a large range which is attributed to local variation due to depletion or enrichment. For example, in northern Lesotho, Letseng le Terae and Liqhobong kimberlites of similar age show very low and very high-water concentration respectively even though they are in close proximity to each other (15 kms) and are attributed to differing metasomatism (Peslier et al., 2012). The temporal variation is evident in the lower water concentration of Group II Premier kimberlite (Ingrin, Grégoire, 2010) as compared to relatively younger group I kimberlites (~90 Ma). The variation with depth has been characterized as a region with water poor olivines at the base of lithosphere as compared to water enrichment at shallower depths (Peslier et al., 2010; Doucet et al., 2014; etc.). While the different studies of Kaapvaal craton kimberlite xenolith NAMs have identified differences in the water concentration they focus primarily on economic kimberlites, particularly those from Republic of South Africa (RSA). In this study we present water content from 11 peridotite xenoliths from 3 uneconomic kimberlites from Lesotho (Matsoku, Thaba Putsoa and Pipe 200) and 1 economic (Bultfontein) kimberlite from RSA and compare the water contents with that of economic kimberlites from literature.

2. Geological setting

The Kaapvaal craton formed and stabilized between 3.7 and 2.6 Ga ago, and it is composed of Archaean greenstone belts and TTG (tonalite-trondhjemite-granodiorite) gneiss complexes intruded by different generations of granitoid plutons. It is bounded in the north by the Late Archean Limpopo belt, which joins the Zimbabwean craton at 2.8–2.5 Ga (de Wit et al., 1992). The Namaqua Natal orogenic belt formed by continental collision and arc accretion bounds the craton to the south. Whereas the 2.0–1.7 Ga Khesi orogenic belt bounds the Kaapvaal craton in the east, and the Lebombo monocline (Donnelly et al., 2012) bounds it in the west.

Between 1.8 Ga and 60 Ma, kimberlite intrusions punctuated the Kaapvaal craton, with main pulses around the Mesozoic (Jelsma et al., 2009). All four kimberlite pipes studied are Group I kimberlites. The Matsoku, Thaba Putsoa, and Pipe 200 kimberlites are in northeastern Lesotho and are part of a geographically isolated cluster of about 60 kimberlites that intruded into the volcanic plateau highlands (Fig. 1). The Lesotho Kimberlite Province is located on the Kaapvaal craton's margin, where Group I kimberlites intrude the Kaavaal craton rocks (Nixon, 1973). The geology of the province consists of Karoo sedimentary rocks capped by Late Jurassic basaltic lavas and associated dolerite intrusions (Skinner, Truswell, 2006). Lesotho Formation is made up of basaltic lavas from the Karoo Supergroup. Bultfontein is part of the Kimberley cluster, which also includes the De Beers, Dutoitspan, Wesselton, Kimberley, and possibly Kamfersdam kimberlites, as well as a number of smaller pipes and sill systems (Field et al., 2008). The cluster is located in the Kaapvaal craton's southwest corner (Fig. 1). The host lithologies are Karoo sedimentary rocks, primarily Dwyka formation shales intruded by Karoo dolerite sills.

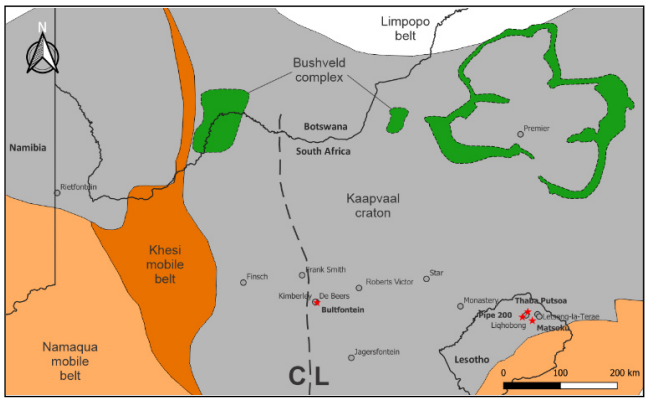

Figure 1 – Geological map of southern Africa showing the outline of the Archean Kaapvaal craton and surrounding Proterozoic terranes and mobile belts
The kimberlites from this study (red star) are shown along with other kimberlites from literature (grey circles); CL: Colesberg Lineament.

3. Materials and methods

All 11 xenolith thick sections are garnet harzburgites with variable amount of primary spinel and clinopyroxene (Table 1). The xenoliths from economic Bultfontein kimberlite (RSA) is affected by shearing and show primary garnets with thin kelyphitic rims. Whereas, the xenoliths from uneconomic kimberlites in norther Lesotho show protogranular texture and are affected by varying degree of metasomatism. The metasomatized garnets are characterized by its breakdown to form assemblage of spinel, phlogopite and clinopyroxene (Table 1). The olivine and orthopyroxene occur as large crystals with smooth curved grain boundaries.

FTIR microscopic analysis was conducted on unoriented samples to study hydrogen distribution and calculate water contents in the NAMs of the 11 selected thick sections. The analysis was carried out at the Institute for Geological and Geochemical Research, Budapest, using Bruker FTIR Vertex 70 spectrometer equipped with a Globar light source and MCT-A detector was coupled to a Bruker Hyperion 2000 microscope and at Budapest University of Technology and Economics, using the Perkin Elmer Spectrum 400 infrared spectrometer along with a coupled Spotlight 400 FTIR imaging system. The double-polished thick sections have a thickness of 256–447 µm (Table 2). The analyses were carried out using unpolarized light. The olivine, pyroxene and garnet measurements were collected between 4000 and 400 cm^{-1}, using an aperture of 50 × 50 µm. The measurements were performed using a 'Globar' light source, a KBr beam splitter and an MCT detector. Both background and sample scans were carried out at 128 scans at 4 cm^{-1} resolutions. The analysis, data correction and processing details are described in Patkó et al. (2019) and Liptai et al. (2021).

Table 1 – Mineral assemblage of the three uneconomic kimberlites from northern Lesotho and economic kimberlite from RSA. The samples with garnet breakdown assemblage (in bracket) are in bold.

Xenolith	Pipe	Assemblage	Metasomatism
26-8A	Matsoku	Ol + Opx + Grt + Di	–
26-8B		**Ol + Opx + Grt + Chr + (Chr + Phl + Di)**	+
26-9		**Ol + Opx + Grt + Phl + (Chr + Phl + Di)**	+
26-16A	Thaba Putsoa	**Ol + Opx + Grt + Chr + (Chr + Phl + Di)**	+
26-16B		**Ol + Opx + Grt + Chr + Di + (Spl + Phl + Di)**	+
26-29A	Pipe 200	Ol + Opx + Grt + Di + Chr	–
26-29B		Ol + Opx + Grt + Di + Chr	–
26-32B		**Ol + Opx + Grt + Chr + (Chr + Phl + Di)**	+
26-32C		**Ol + Opx + Grt + Di + Chr + Phl + (Chr + Phl + Di)**	+
51	Bultfontein	Ol + Opx + Grt + Di + Chr	–
55A		Ol + Opx + Grt + Chr	–

4. Results

The olivine absorption peaks are in Group 1 region of OH infrared absorption bands (3415–3653 cm^{-1}). It is calculated using at least five differently oriented grains. The suggest hydrogenation pressure of Group 1A (P >2 GPa) (Matveev, Stachel, 2007) with the main and highest absorbance at ~ 3571 cm^{-1}. The subsequent absorption band is at ~3591 cm^{-1} except in the Pipe 200 xenoliths where the peak at ~3638 cm^{-1} has higher absorbance than the one at ~3591 cm^{-1}. One of the two Bultfontein xenolith's (51) olivine shows characteristic broad peak at 3324 cm^{-1} which is controlled by elevated water or hydrogen fugacity (Matveev, Stachel, 2007). Other absorption bands are at ~3624, ~3612, ~3638, ~3534 cm^{-1}. The peak at ~3534 cm^{-1} is characteristic of H in a Ti-clinohumite point defect (Berry et al., 2005). Extreme care was taken to not measure serpentine, the data was checked for ~3690 cm^{-1} serpentine peak. Profile measurement carried out on olivine grains are flat and do not show diffusion profiles. The calculated water concentration is tabulated in Table 2 with 41–62 ppm in Bultfontein, 24–27 ppm in Matsoku, 25–30 ppm in Thaba Putsoa and 17–33 ppm in Pipe 200 kimberlite.

All orthopyroxenes show absorption band at ~3515, ~3540, and a broad band at ~3596–3600 cm^{-1}. However, the Pipe 200 xenoliths affected by metasomatism have the dominant peak at ~3590 cm^{-1}. Other low intensity peaks include broad peaks at ~3400, ~3310 and ~3055 cm^{-1}. The high intensity peak at 3690 with asymmetric shoulder is due to serpentine (Post, Borer, 2000). The water concentration is calculated using a single or two to three differently oriented orthopyroxene crystals. However, it may be underestimated because of removal of serpentine peaks, especially in the xenoliths from Pipe 200. The calculated water concentration shows a large variation 21–230 ppm (Table 2) with the xenoliths from Pipe 200 having the lowest orthopyroxene water concentration at 41–94 ppm.

Table 2 – Calculated water concentration in the NAMs from the three uneconomic kimberlites from northern Lesotho and economic kimberlite from RSA. The samples with garnet breakdown assemblage due to metasomatism are in bold.

Xenolith	Thickness	Olivine		Orthopyroxene		Clinopyroxene		$D_{H2O}^{opx/ol}$
		Absorbance	H_2O ppm	Absorbance	H_2O ppm	Absorbance	H_2O ppm	
26-8A	447	2.2	27	20.9	94	9.3	87	3.5
26-8B	**388**	**1.7**	**24**	**22.0**	**115**	**30.6**	**331**	**4.7**
26-9	**446**	**–**	**–**	**32.0**	**145**	**48.8**	**460**	**–**
26-16A	**427**	**2.3**	**30**	**26.3**	**125**	**–**	**–**	**4.1**
26-16B	**385**	**1.7**	**25**	**43.6**	**230**	**–**	**–**	**9.1**
26-29A	429	2.5	33	19.6	92	–	–	2.8
26-29B	377	1.8	27	8.3	45	66.1	737	1.7
26-32B	**256**	**0.9**	**20**	**–**	**–**	**–**	**–**	**–**
26-32C	**286**	**0.9**	**17**	**3.0**	**21**	**56.8**	**833**	**1.2**
51	425	3.1	41	36.8	175	61.1	604	4.3
55A	379	4.1	62	11.3	60	–	–	1.0

Clinopyroxene shows broad absorption peaks at ~3634–3640, ~3450–3452 cm^{-1}. Only Bultfontein xenolith shows an additional peak at ~3570 cm^{-1}. The calculated clinopyroxene water concentration (87–833 ppm) is slightly overestimated and higher than that reported in literature. The Pipe 200 xenoliths have the highest water concentration whereas the Matsoku xenoliths have lower water concentration with samples having unmetasomatized garnet having lowest water concentration (87 ppm). The garnets show only bands associated with contamination and are assumed to be dry.

5. Discussion

The measured olivine water concentration is between 17–62 ppm (Table 2). It is in the 0–86 ppm range reported in Peslier et al. (2008, 2010) for Kaapvaal craton xenoliths. The economic (Bultfontein) kimberlite has higher water content (41, 62 ppm) as compared to uneconomic kimberlites from northern Lesotho (17–33 ppm). Within the xenoliths from northern Lesotho, the ones affected by metasomatism (phlogopite + spinel + diopside assemblage) has lower olivine water content than those with primary garnets. Furthermore, the flat diffusion profiles in all the olivine when combined with the low water absorbance in the uneconomic kimberlites hint towards its diffusion and re-equilibration. The orthopyroxene water concentration of 21–230 ppm covers a large range and falls well within that (40–250 ppm) of the Kaapvaal craton peridotite xenoliths measured in Peslier et al. (2012). The serpentine peak at ~3690 cm^{-1} affects the orthopyroxene water concentration and it is underestimated. In the Matsoku orthopyroxene which are unaffected by serpentine the xenoliths with garnet breakdown assemblage have higher water concentration as compared to those with primary garnets. The water concentration in clinopyroxene covers a large range (87–833 ppm) and is higher than that (150–400 ppm) mentioned in Peslier et al. (2012). This higher water concentration is due to overestimation due to removal of serpentine.

In all the xenoliths affected by metasomatism, the olivine has lower water concentration than those with primary garnets. In the case of Matsoku xenoliths, both orthopyroxene and clinopyroxene (unaffected by serpentine) show higher water concentration in those with metasomatic garnet breakdown assemblage. The olivine and to an extent orthopyroxene water concentration in the economic kimberlite (Bultfontein) is higher as compared to the uneconomic kimberlites from northern Lesotho. The ratio of water contents in orthopyroxene and olivine (inter-mineral H_2O partition coefficient) is calculated to be 1.6 ± 0.2 for megacrysts from Kaapvaal craton (5 GPa) by Bell et al. (2004) and 0.61 by Withers et al. (2011) (6 GPa). The calculated $D_{H2O}^{opx/ol}$ is higher and goes up to 9.1 for uneconomic kimberlites and 4.3 for economic Bultfontein kimberlite. The $D_{H2O}^{opx/ol}$ is higher than that mentioned in literature.

The distribution of water concentration between the olivine and orthopyroxene when compared with the data from literature (Bell, Rossman 1992; Kurosawa et al., 1997; Peslier, 2010; Grant et al., 2007; Baptiste et al., 2012; Peslier et al., 2012, 2017; Schmädicke et al., 2013; etc.) in Figure 2 highlights the overall lower olivine water content of economic kimberlites. Furthermore, when compared with the equilibration pressure of these xenoliths from literature, they define two different trends defined by lower (<5 GPa) and higher (>5 GPa) pressures with the higher-pressure kimberlites having lower olivine water content. This observation is similar to that of enrichment of shallower mantle by fluids and melt and dry metasomatism at the base of lithospheric mantle. All the studied xenoliths fall within the lower pressure range where the difference between the economic and uneconomic kimberlites is evident (Fig. 2) with the uneconomic kimberlites having lower orthopyroxene water concentration as compared to the economic kimberlites representing the same shallower mantle (<5 GPa). Therefore, the metasomatic events at higher pressure have resulted in the removal of water in the olivine at higher pressure. However, despite the enrichment the uneconomic kimberlites have lower orthopyroxene content.

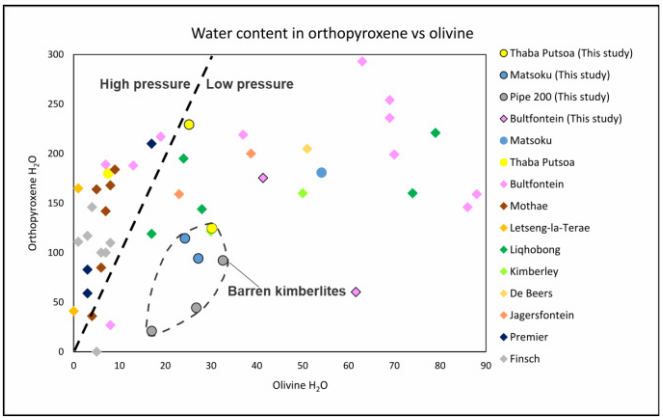

Figure 2 – Orthopyroxene vs olivine water concentration in the economic (rhombus) and uneconomic (circles) kimberlites from the Kaapvaal craton from this study (black outline) compared with those from literature (no outline)

References

Baptiste, V., Tommasi, A., Demouchy, S. (2012): Lithos, **149**, 31–50.

Bell, D.R., Rossman, G.R. (1992): Science (New York, N.Y.), **255/5050**, 1391–1397.

Bell, D.R., Rossman, G.R., Moore, R.O. (2004): Journal of Petrology, **45/8**, 1539–1564.

Berry, A.J., Hermann, J., O'Neill, H.S.C., Foran, G.J. (2005): Geology, **33**, 869–872.

de Wit, M.J., de Ronde, C.E.J., Tredoux, M., Roering, C., Hart, R.J., Armstrong, R.A., Green, R.W.E., Peberdy, E., Hart, R.A. (1992): Nature, **357**, 553–562.

Donnelly, C.L., Griffin, W.L., Yang, Jin-H., O'Reilly, S.Y., Li, Qiu-L., Pearson, N.J., Li, Xian-H. (2012): Journal of Petrology, **53/12**, 2497–2522.

Doucet, L.S., Peslier, A.H., Ionov, D.A., Brandon, A.D., Golovin, A.V., Goncharov, A.G., Ashchepkov, I.V. (2014): Geochimica et Cosmochimica Acta, **137**, 159–187.

Fedortchouk, Y., Canil, D., Semenets, E. (2007): American Mineralogist, **92**, 1200–1212.

Field, M., Stiefenhofer, J., Robey, J., Kurszlaukis, S (2008): Ore Geology Reviews, **34/1–2**, 33–75.

Grant, K., Ingrin, J., Lorand, J.P., Dumas, P. (2007): Contributions to Mineralogy and Petrology, **154/1**, 15–34.

Ingrin, J., Grégoire, M. (2010): EGU General Assembly Conference 12, 13028

Jelsma, H., Barnett, W., Richards, S., Lister, G (2009): Lithos, **112**, 155–165.

Khokhryakov, A., Palyanov, Y. (2010): American Mineralogist, **95/10**, 1508–1514.

Kovács, I., Hermann, J., O'Neill, H.S.C., Gerald, J.F., Sambridge, M., Horvath, G. (2008): American Mineralogist, **93**, 765–778.

Kurosawa, M., Yurimoto, H., Sueno, S. (1997): Physics and Chemistry of Minerals, **24**, 385–395.

Liptai, N., Lange, T.P., Patkó, L., Pintér, Z., Berkesi, M., Aradi, L.E., Szabó, C., Kovács, I.J. (2021): Global and Planetary Change, **196**, 103364

Matveev, S., Stachel, T. (2007): Geochimica Et Cosmochimica Acta, **71**, 5528–5543.

Nixon, P.H. (Ed) (1973): Lesotho Kimberlites, Lesotho National Development Corporation, 48–56.

Patkó, L., Liptai, N., Kovács, I.J., Aradi, L.E., Xia, Q. Ingrin, J., Mihály, J., O'Reilly, S.Y., Griffin, W.L., Wesztergom, V., Szabó, C. (2019): Chemical Geology, **507**, 23–41.

Peslier, A.H. (2010): Journal of Volcanology and Geothermal Research, **197/1–4**, 239–258.

Peslier, A.H., Woodland, A.B., Wolff, J.A. (2008): Geochimica et Cosmochimica Acta, **72**, 2711–2722.

Peslier, A.H., Woodland, A.B., Bell, D.R., Lazarov, M. (2010): Nature, **467/7311**, 78–81.

Peslier, A.H., Woodland, A.B., Bell, D.R., Lazarov, M., Lapen, T.J. (2012): Geochimica et Cosmochimica Acta, **97**, 213–246.

Peslier, A.H., Schönbächler, M., Busemann, H., Karato, S.-I. (2017): Space Science Reviews, **212/1**, 743–810.

Post, J.L., Borer, L. (2000): Applied Clay Science, **16/1–2**, 73–85.

Schmädicke, E., Gose, J., Witt-Eickschen, G., Brätz, H. (2013): American Mineralogist, **98/10**, 1870–1880.

Skinner, E.M.W., Truswell, J.F. (2006): In: Johnson, M.R., Anhaeusser, C.R., Thomas, R.J. (Eds.): The geology of South Africa, Geological Society of South Africa and Council for Geoscience, Johannesburg, Pretoria, 651–659.

Withers, A.C., Hirschmann, M.M., Tenner, T.J. (2011): American Mineralogist, **96/7**, 1039–1053.